Contributions to Geophysics and Geodesy Vol. 45/2, 2015 (135–148)

2D density model of the Chinese continental lithosphere along a NW-SE transect

Barbora ŠIMONOVÁ[1], Miroslav BIELIK[1,2], Jana DÉREROVÁ[2]

[1] Department of Applied and Environmental Geophysics, Faculty of Comenius University, Mlynská dolina, Ilkovičova 6, 842 48 Bratislava, Slovak Republic; e-mail: bielik@fns.uniba.sk

[2] Division of Geophysics, Earth Science Institute of the Slovak Academy of Sciences, Dúbravská cesta 9, 845 28 Bratislava, Slovak Republic; e-mail: geofmiro@gmail.com

Abstract: This paper presents a 2D density model along a transect from NW to SE China. The model was first constructed by the transformation of seismic velocity to density, revealed by previous deep seismic soundings (DSS) investigations in China. Then, the 2D density model was updated using the GM-SYS software by fitting the computed to the observed gravity data. Based on the density distribution of anomalous layers we divided the Chinese continental crust along the transect into three regions: north-western, central and south-eastern. The first one includes the Junggar Basin, Tianshan and Tarim Basin. The second part consists of the Qilian Orogen, the Qaidam Basin and the Songpan Ganzi Basin. The third region is represented by the Yangtze and the Cathaysia blocks. The low velocity body (v_p = 5.2 – 6.2 km/s) at the junction of the North-western and Central parts at a depth between 21 – 31 km, which was discovered out by DSS, was also confirmed by our 2D density modelling.

Key words: gravity, deep seismic sounding, density, seismic velocity, modelling, continental crust, China

1. Introduction

The global tectonic mechanism controls the movement of the lithospheric plate. The dynamic movement also affects evolution of the Chinese continent. The Indian plate separated from Antarctic plate nearly 200 Ma ago, at about the same time South America and Africa separated. The Indian plate moved to the north by closing the Tethys Ocean. The collision between the Indian and Eurasian plates occurred in Paleogene, at about 55 Ma, at about 5 cm per year. This significant movement of two colliding

doi: 10.1515/congeo-2015-0017

continental plates caused an extremely strong collision resulting in the Himalayas, uplift of the Tibetan Plateau and hundreds of kilometres of crustal displacement to the east and southeast (*Winn, 2012*). The Chinese region has attracted the attention of the scientific community because of its great importance for understanding the structure, composition and dynamics of the continental lithosphere (e.g., *Chen et al. 2009, 2010, 2013, 2015; Li et al. 2008; Zhang et al. 2004, 2008, 2009, 2010*).

To contribute to this study, the main topic of this paper is investigation of crustal density in the Chinese mainland. The crustal structure along the transect was constrained by seismic velocity profiles published by *Zhang et al. (2011)*. For determination of the resultant 2D density model, the GMSYS software has been applied to fit the gravity data between the computed and the observed.

2. Geology setting

In China, there are three platforms: the Tarim platform (Northwest), the Yangtze platform (South) and the North China platform (North). In addition, the continental domain and the adjacent oceanic areas are formed by three major fold tectonic units, which are represented by the Tethyan-Himalayan zone (Southwest), the Paleo-Asian zone (North) and the Circum-Pacific zone (East). These fold tectonics units are subdivided into fifteen fold systems (Fig. 1, *Zhang et al., 2011*).

The transect of this study extends from Altai, located in the Northwest of China, to Quanzhou in the Southeast of China (Fig. 1). From its beginning to the end it intersects the following tectonic units: the Junggar Basin, Tianshan, Tarim Basin, Qilian Orogen, Qaidam Basin, Songpan-Ganzi and South China Block.

The Junggar Basin is situated in Northwest China. It lies between the Altai orogeny in the southern part of the Siberian plate, Kazakhstan plate and Tianshan fold system. The basin is a late Paleozoic, Mesozoic and Cenozoic compressional superimposed basin, experienced by several orogenies (*Chen et al., 2002*).

The Tianshan is defined to the north by the Junggar Basin and the southern Kazakhstan plains and to the southeast by the Tarim Basin (*Encyclopædia Britannica, 2015b*). Its topography is considered to be the result of

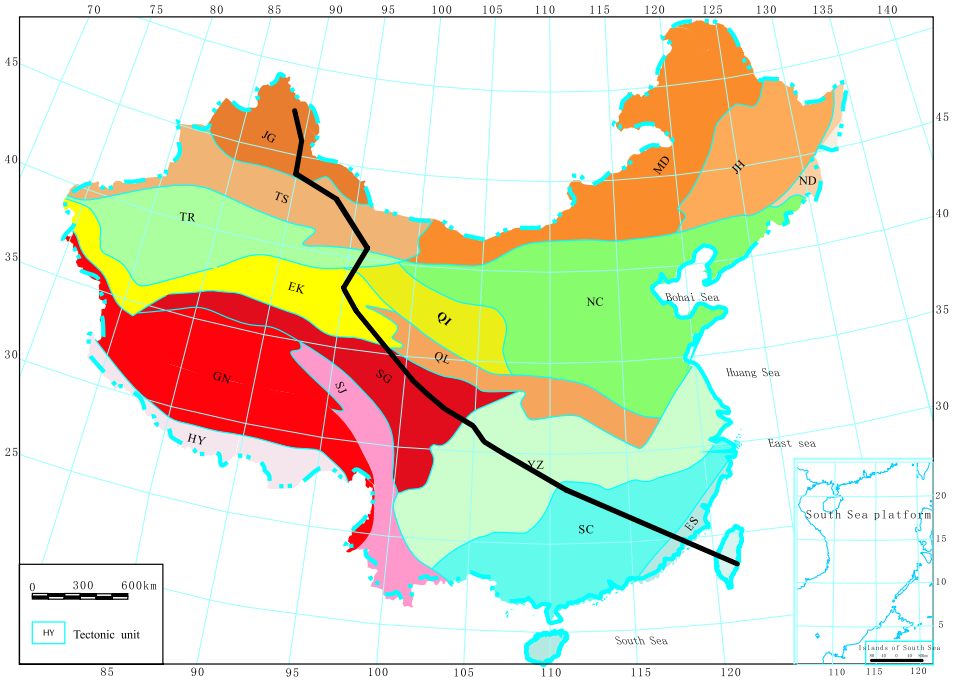

Fig. 1. Location of the transect on the schematic tectonic map (after *Zhang et al., 2011*). Keys: Platforms: TR – Tarim platform, YZ – Yangtze platform, NC – North China platform; Fold systems: JG – Junggar fold system, TS – Tianshan fold system, EK – East Kunlun fold system, QI – Qilian fold system, SG – Songpan Ganzi fold system, GN – Gangdise Nyainqentanglha fold system, SJ – Sanjiang fold system, HY – Himalayan fold system, MD – Mongolia-Daxinganlin fold system, JH – Ji He fold system, ND – Nadanhada fold system, QL – Qinling fold system, SC – South China fold system, SA – Sea area.

crustal shortening related to the ongoing Indian-Eurasian collision that started in the early Tertiary. This range belongs to the largest Central Asian Orogenic Belt (*Jolivet et al., 2010*). The Tianshan Mts. are composed of Paleozoic crystalline rocks and the basins are filled with younger sediments (*Encyclopædia Britannica, 2015b*).

The Tarim Basin is the largest sedimentary basin in China (*Li et al., 2004*). Its vast depression is located in the Xinjiang region (northwestern China). The basin is enclosed by the Tianshan Mts. (North), Pamir Mts. (West), Kunlun Mts. (South) and Altyn Mts. (East) (*Encyclopædia*

Britannica, 2015a). The basin contains sediments of Cambrian to Tertiary ages. The sedimentary environment evolved from a Paleozoic marine carbonate platform, through fluvial environment in the Mesozoic and the Cenozoic. These sediments overlie the Archean and the Proterozoic crystalline basement (*Xiang et al., 2013*).

The Qilian Orogen records the early-middle Paleozoic collision between the Qaidam Block to the south and the North China Craton to the north. The orogeny is fault bound and is separated from the Tarim Block to the west by the Altyn Tagh Fault and from the North China Craton to the north and east by the Longshoushan and Tongxin-Guyuan faults, respectively. From the Qaidam Block to the south it is separated by a series of thrust faults (*Yang et al., 2012*). The orogeny is subdivided into three units: the North, Central and South Qilian Belts. In the North Qilian Belt the volcano-sedimentary basin has been created during the Cambrian to Devonian. The basin is filled with siliciclastic rocks and carbonates. The Central Qilian Block is composed mainly of Proterozoic granitic gneiss and siliciclastic and carbonate metasedimentary rocks. Lithological units include Cambrian-Ordovician lava flows, pyroclastic rocks, Silurian flysch, and the ultrahigh-pressure metamorphic rocks (*Yang et al., 2012*).

The Qaidam Basin is a large and almost flat region at the north-eastern margin of the Tibetan Plateau (*Mischke et al., 2006*). It is a composite sedimentary basin developed on typical continental crust and comprises a Jurassic foreland basin and a Cenozoic extensional basin. The evolution of the basin is a result of two mega stages. The first mega stage (from latest Cretaceous to Oligocene) consisted of two periods of rifting due to upwelling of the hot upper mantle. The second stage comprised three tectono-sequences that developed in the Miocene and Pliocene and was a period of structural inversion that consisted of compressive down-warping and reverse faulting caused by collisions of the Indian and Eurasian plates (*Xia et al., 2001*).

The Songpan-Ganzi Basin is located on the southwestern flank of the Central China Orogenic Belt on the northeast corner of the Tibetan Plateau. It is the most extensive area of exposed Triassic sedimentary rocks on Earth (*She et al., 2006*). The basin is filled by flysch sediments, the major source rocks of which come from the surrounding magmatic and orogenic belts. Songpan-Ganzi has been interpreted as a remnant ocean basin between the colliding south and north China blocks, as a Permian-Triassic rift basin,

and as a back-arc basin (*Enkelmann et al., 2007*).

The South China Block is located in southeast China. It is composed of two blocks, Cathaysia and Yangtze, which have been considered as two separate parts of the Neoproterozoic Rodinia supercontinent. Cathaysia is separated from the Yangtze block by a Neoproterozoic ophiolitic suture along the Shaoxing–Jiangshan–Pingxiang fault due to collision between the two blocks during the early Neoproterozoic, around 900 Ma (*Shu et al., 2011*).

3. Input data and methodology

The interpreted transect has a length of 4575 km and extends to a depth of 80 km. The input data are represented by topography and bathymetry (Fig. 2) (from GTOPO30 data set (*Gesch et al., 1999*) and the total Bouguer gravity data (Fig. 2), which has been extracted along the transect from the Bouguer anomaly map of the Chinese mainland (*Yuan, 1989*). The input 2D density model has been constructed based on the seismic velocities revealed by previous DSS investigations (Fig. 3, *Zhang et al., 2011*). The densities of the anomalous bodies have been calculated by transformation of the seismic velocities v_p to densities by Csicsay's formula (*Csicsay et al., 2012*, Table 1). This formula is a linear approximation of the Sobolev-Babeyko's equation (*Sobolev and Babeyko, 1994*).

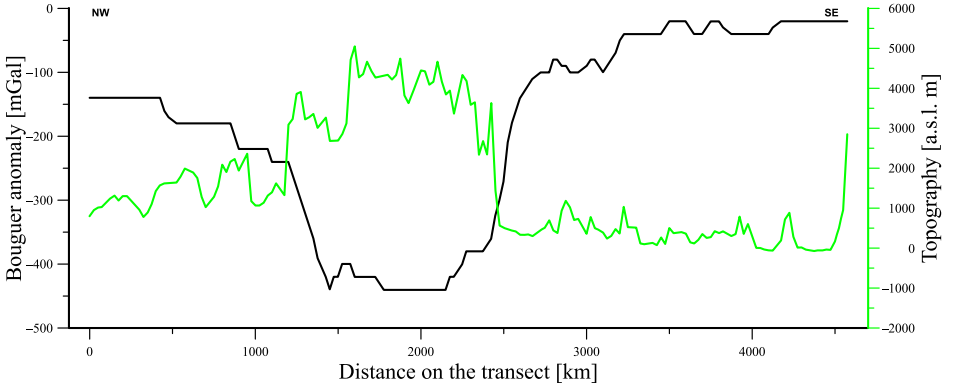

Fig. 2. Total Bouguer anomaly *(Yuan, 1989)*, and Topography and Bathymetry in sea area (from GTOPO30 data set (*Gesch et al., 1999)*).

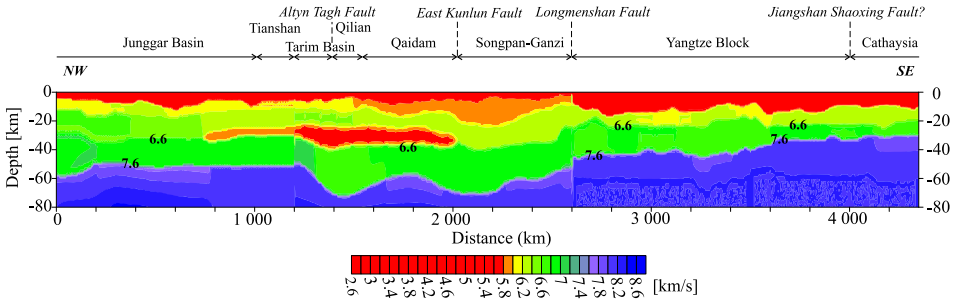

Fig. 3. P-wave velocity structure along the transect in China (after *Zhang et al., 2011*).

The topography and bathymetry of the transect is very rugged. It varies from −70 m to +5067 m a.s.l. From northwest to southeast, the topography in the first third of the transect is about 1000 m a.s.l. on average, in the central part it is the highest (3000 m a.s.l. on average) and in the last third the topography has an average of about 500 m a.s.l., except for the Taiwan Strait and Taiwan island.

The total Bouguer anomaly values range from −440 to −20 mGal. The sig- nificant gravity minimum can be observed in the central part of the transect. Note that this gravity minimum correlates very well with the highest topography, which is typical for the collision orogens (e.g., *Lillie, 1991*). From this area the gravity values gradually increase, reaching about −200 mGal in the Northwestern part and about −50 mGal in the Southeast on average.

Table 1. Transformation of seismic velocity v_p to densities using Csicsay's formulae (*Csicsay et al., 2012*).

v_p [km/s]	ρ [kg/m^3]
5.0	2 190
5.2	2 280
5.6	2 460
5.8	2 550
6.0	2 640
6.08	**2 680**
6.13	**2 700**
6.16	**2 710**
6.18	**2 720**
6.2	2 730
6.4	2 820
6.6	2 910
6.8	**3 000**
7.0	**3 100**
7.2	3 190
7.3	**3 230**
7.4	3 280
7.55	3 350
7.6	3 370
7.7	**3 410**
7.8	3 460
8.0	3 550

The P-wave velocities along the transect (Fig. 3) were constructed by *Zhang et al. (2011)*. The v_p values range from 4.6 to 8.6 km/s. The Moho depth varies from 30 km to about 72 km. It is worth mentioning the existence of a significant crustal low velocity layer (LVL) between distances of 650 km and 2000 km at an approximate depth of 30 km.

The quantitative interpretation of the observed gravity along the transect was carried out by application of the software GM-SYS (*GM-SYS User's Guide for version 4.9, 2004*). The program is capable of interactive gravity and magnetic interpretations. The calculations of the gravitational effects of the geological bodies are based on the formulae defined by *Talwani et al. (1959)*, with Won and Bevis's algorithm (*GM-SYS User's Guide 4.9, 2004*). The model results were modified by trial and error until a reasonable fit was obtained between the measured and calculated gravity data. In this study, the deviation between gravitational effect and observed gravity reaches only ± 10.4 mGal.

4. Results

The resultant model (Fig. 4) consists of eleven density anomalous layers, of which the average densities vary from $1030 - 3400$ kg/m^3. Generally, the density increases with depth. The uppermost part of the crust is composed of a layer with the average density 2670 kg/m^3. Its thickness varies significantly along the transect. In the North-western segment of the transect it attains a thickness of 10 km, while the central part is thinner (4 km on average). This medium has the largest thickness in the South-eastern segment of the transect. It is 12 km on average, with the thickness increasing by 10 km at the end of the transect. Note that the thickness of this uppermost layer changes extremely at the junction of the central and South-eastern part. This noticeable feature of the gravity field correlates very well with the deep-seated course of the Longmenshan fault (*Zhang et al., 2009, 2010*).

The density layer 2700 kg/m^3 is located under the uppermost layer. It can be observed in the South-western sector of the transect and partly in the Central and North-eastern part. In the central part of the transect, density inhomogeneities with density 2680 kg/m^3 are located above this very thin layer. The thickness of this layer reaches up to 20 km in some

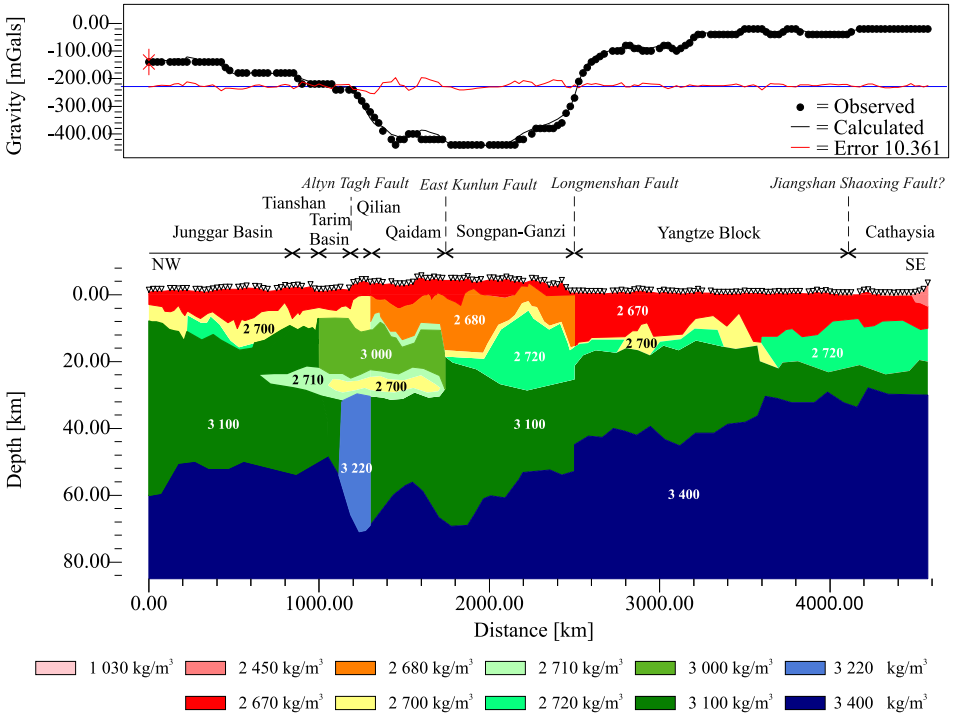

Fig. 4. Resultant density model of the transect in China.

places. The lower part of the upper crust is formed by inhomogeneities with average densities of 2710 – 2720 kg/m^3. The largest one (2720 kg/m^3) can be seen in the Central part at the depth of about 20 km. The thickness of this body reaches 20 km. Its centre is at km 2100 of the profile. In the South-eastern part of the transect inhomogeneity (layer) of this density has a thickness of 10 – 12 km. In the depths of about 7 – 28 km we modelled a density heavy body (3000 kg/m^3). Its average thickness is about 12 km. Under this layer (in the bottom of the lower crust) a low density layer (2700 – 2710 kg/m^3) was interpreted. This body correlates very well with the interpreted low velocity seismic layer by *Zhang et al. (2011)*. Both mentioned anomalous layers are situated in the wider border among the North-western and Central parts (1000 – 1700 km). The whole lower crust is built by a layer with a density of 3100 kg/m^3, except for a vertical den-

sity inhomogeneity (3220 kg/m^3), which is located in the part transect of 1115 – 1300 km in a depth of 30 – 71 km. Note that we doubt if this vertical density body is real. The upper mantle is characterized by an average density of 3400 kg/m^3. The depth of the Moho varies from 28 km to 71 km. Its gravitational effect was also determined and it is shown in Fig. 5c. It can be concluded that this effect reflects naturally the Moho course. The largest gravitational effect is in places in which the Moho boundary has the largest depth. Generally, the effect increases from the North-western to the South-eastern parts of the transect. It is due to the decreasing of Moho. To determine the relative gravitational effects of topography and crust for the total gravity we also calculated their gravitational effects (Fig. 5a,b).

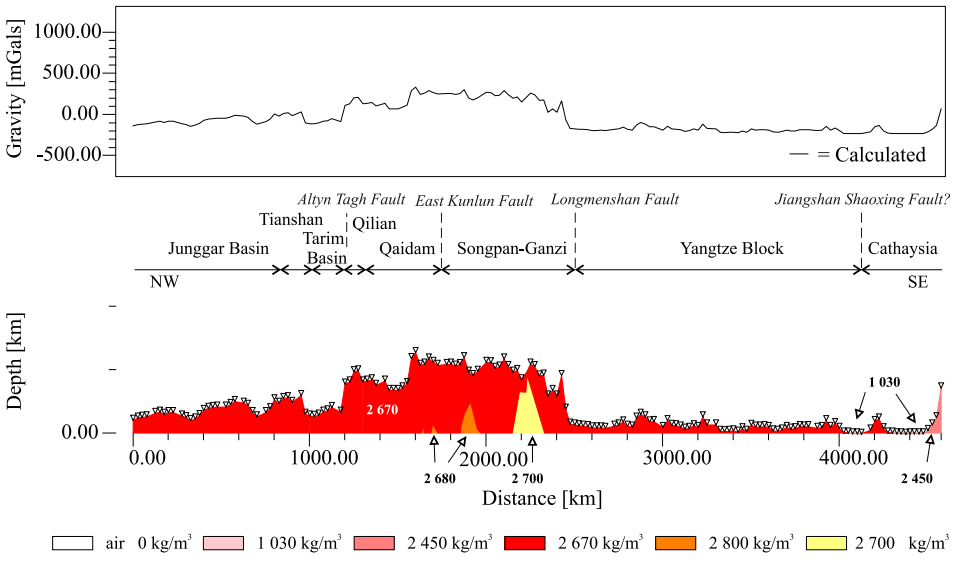

Fig. 5a. Gravitational effects of topography.

It is also worth noting that the Altyn Tagh, East Kunlun, Longmenshan and Jiangshan Shaoxing faults are observable in the resultant 2D density model. Distribution of the density bodies within the whole crust indicates clearly the faults are deep-seated. Specifically, the Altyn Tagh fault and Longmenshan fault are clearly traceable.

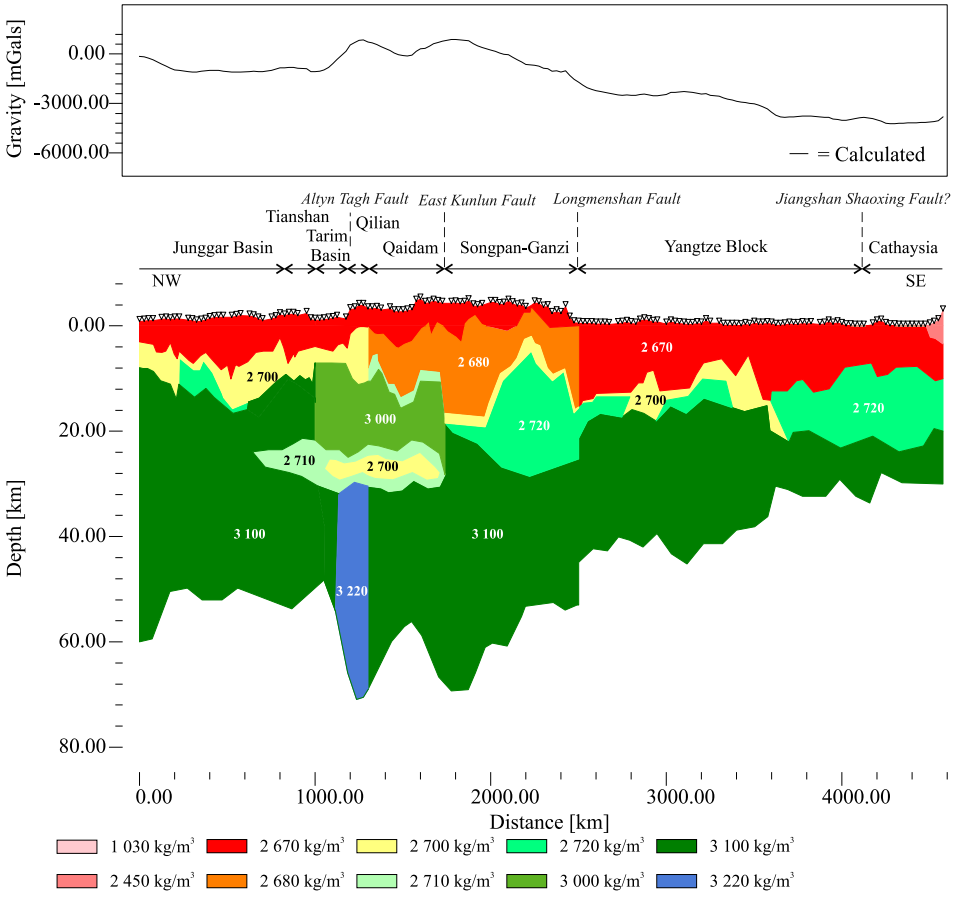

Fig. 5b. Gravitational effects of crust.

5. Conclusion

Based on the interpretation of gravity field along the transect we divide the continental crust into three regions: North-western, Central and South-eastern parts. The North-western part is separated from the Central one by the Altyn Tagh fault, while the Longmenshan fault divides the Central and the South-eastern parts. The resultant density model shows clearly that the structure of the crust varies considerably in all three sections. The first one

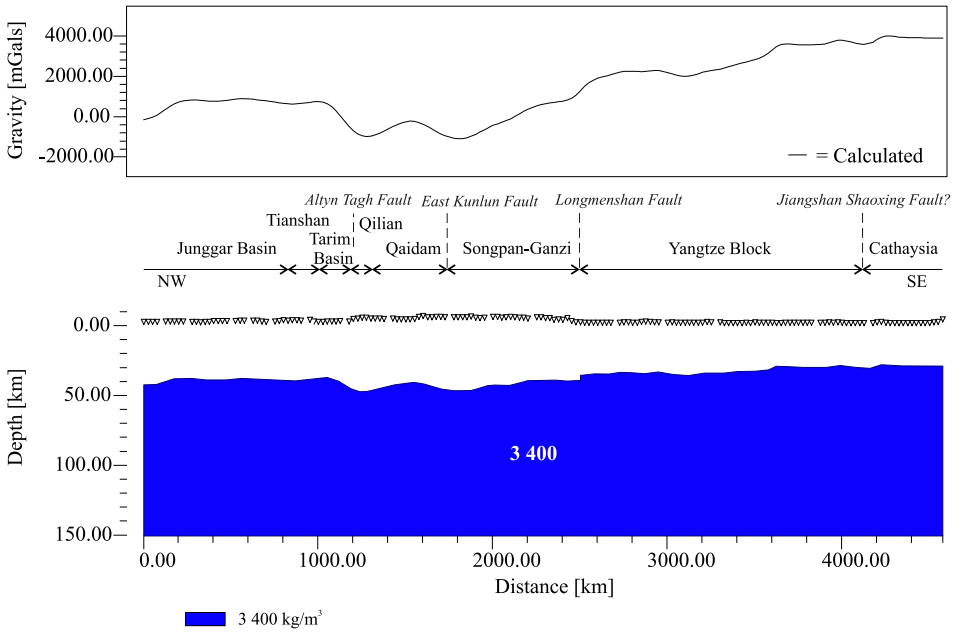

Fig. 5c. Gravitational effects of upper mantle.

includes the Junggar Basin, Tianshan and Tarim Basin and it is characterized by gravity values from about –140 mGal to –240 mGal, topography (1500 m a.s.l. on average) and average crustal thickness of 50 km. The central part consists of the Qilian Orogen, Qaidam Basin and Songpan-Ganzi block. In this region the extreme values (> 5000 m) of topography (3600 m a.s.l. on average) and the Moho depth (average value is about of 64 km) and gravity (> -400 mGal) can be observed. The Moho depth has two minima, which reach the maximum depth of 72 km and 70 km, respectively. The last one is represented by the Yangtze and the Cathaysia blocks. These blocks have very low topography (500 m a.s.l. on average), except for the Taiwan Strait and Taiwan Island. By comparing the v_p velocity profile (*Zhang et al., 2011*) with our resultant density model, it was shown that they are in good agreement. It is also supported, for example, by the feature that the LVL ($v_p = 5.2 - 6.2$ km/s) at the junction between the North-western and Central parts at a depth between $21 - 31$ km (*Zhang et al., 2011*) was also revealed and confirmed by 2D density modelling.

Acknowledgments. We thank Prof. Zhongjie Zhang for his provision of the seismic velocity structure along the transect in China. This research has been supported by the Slovak Research and Development Agency, grant No. APVV-0724-11 and the Slovak Grant Agency VEGA, grants No. 1/0141/15, and No. 2/0042/15.

References

Chen X., Lu H. F., Shu L. S., Wang H. M., Zhang G. Q, 2002: Study on tectonic evolution of Junggar Basin. Geological Journal of China Universities, **8**, 3, 257–267.

Chen Y., Badal J., Zhang Z. J., 2009: Radial anisotropy in the crust and upper mantle beneath the Qinghai-Tibet plateau and surrounding regions. Journal of Asian Earth Sciences, **36**, 289–302.

Chen Y., Badal J., Hu J. F., 2010: Love and Rayleigh wave tomography of the Qinghai-Tibet Plateau and surrounding areas. Pure and Applied Geophysics, **167**, 1171–1203.

Chen Y., Zhang Z. J., Sun C. Q., Badal J., 2013: Crustal anisotropy from Moho converted Ps wave splitting analysis and geodynamic implications beneath the eastern margin of Tibet and surrounding regions. Gondwana Research, **24**, 946–957.

Chen Y., Li W., Yuan X. H., Badal J., Teng J. W., 2015: Tearing of the Indian lithospheric slab beneath southern Tibet revealed by SKS-wave splitting measurements. Earth and Planetary Science Letters, **413**, 13–24.

Csicsay K., Bielik M., Mojzeš A., Spováková E., Kytková B., Grinč M., 2012: Linearization of the Sobolev and Babeyko's formulae for transformation of P-wave velocity to density in the Capathian-Pannonian Basin region. Contrib. Geophys. Geod., **42**, 1, 15–23.

Encyclopædia Britannica, 2015a: Tarim Basin. Online. Retrieved 11 September, 2015, from <http://www.britannica.com/place/Tarim-Basin>.

Encyclopædia Britannica, 2015b: Tien Shan. Online. Retrieved 11 September, 2015, from <http://www.britannica.com/place/Tien-Shan>.

Enkelmann E., Weislogel A., Ratschbacher L., Eide E., Renno A., Wooden J., 2007: How was the Triassic Songpan-Ganzi basin filled? A provenance study. Tectonics, **26**, 4, 1–24.

Gesch D. B., Verdin K. L., Greenlee S. K., 1999: New land surface digital elevation model covers the Earth, Eos Trans. AGU, **8**0, 69–70.

GM-SYS® User's Guide for version 4.9, 2004: Northwest Geophysical Associates, Inc., Corvallis, 101.

Jolivet M., Dominguez S., Charreau J., Chen Y., Li Y., Wang Q., 2010: Mesozoic and Cenozoic tectonic history of the central Chinese Tian Shan: Reactivated tectonic structures and active deformation. Tectonics, **29**, 6, 1–30.

Li D. S., Liang D. G., Jia C. Z., Wang G., Wu Q. Z., He D. F., 2004: Hydrocarbon accumulations in the Tarim Basin, China. AAPG Bulletin, 80, 10, 1587–1603.

Li C., van der Hilst, R., Meltzer A. S., Engdahl E. R., 2008: Subduction of the Indian lithosphere beneath the Tibetan Plateau and Burma. Earth and Planetary Science Letters, **274**, 157–168.

Lillie J. R., 1991: Evolution of gravity anomalies across collisional mountain belts: dues to the amount of continental convergence and underthrusting. Tectonics, **10**, 672–687.

Mischke S., Herzschuh U., Sun N., Qiao Z., Sun Z., 2006: A large Middle Pleistocene freshwater to oligohaline lake in the contemporary hyperarid Qaidam Basin (China). Episodes Journal of International Geoscience, **29**, 1, 34–38.

She Z., Ma Ch., Mason R., Li J., Wang G., Lei Y., 2006: Provenance of the Triassic Songpan-Ganzi flysch, west China. Chemical Geology, **231**, 159–175.

Shu L. S., Faure M., Yu J. H., Jahn B. M, 2011: Geochronological and geochemical features of the Cathaysia block (South China): New evidence for the Neoproterozoic breakup of Rodinia. Elsevier. Precambrian Research, **187**, 3–4, 263–276.

Sobolev S., Babeyko A. Y., 1994: Modeling of mineralogical compositions, density and elastic waves velocity in anhydrous magmatic rocks. Surveys in Geophysics, **15**, 515–544.

Talwani M., Worzel J. L., Landisman M., 1959: Rapid gravity computations for two-dimensional bodies with application to the Mendocino submarine fracture zone. J. Geophys. Res., **64**, 49–59.

Winn P., 2012: Geology and Geography of Tibet and Western China. Online. Retrieved 11 September, 2015, from <http://www.shangri-la-river-expeditions.com/wchinageo/wchinageo.html>.

Xia W., Zhang N., Yuan X., Fan L., Zhang B., 2001: Cenozoic Qaidam Basin, China: A Stronger Tectonic Inversed, Extensional Rifted Basin. AAPG Bullentin, **85**, 4, 715–736.

Xiang C., Pang X., Danišík M., 2013: Post-Triassic thermal history of the Tazhong Uplift Zone in the Tarim Basin, Northwest China: Evidence from apatite fission-track thermochronology. Geoscience Frontiers, **4**, 6, 743–754.

Yuan X. C. (Ed.), 1989: Atlas of Geophysics in China. Publication No. 201 of International Lithosphere Program. Geological publishing House, Beijing, 68.

Yang J. H., Du Y. S., Cawood P. A., Xu Y. J., 2012: From subduction to collision in the northern Tibetan plateau: Evidence from the early Silurian clastic rocks, northwestern China. Journal of Geology, **120**, 1, 49–67.

Zhang P. Z., Shen Z. K., Wang M., Gan W. J., Bürgmann R., Molnar P., Wang Q., Niu Z. J., Sun J. Z., Wu J. C., Sun H. R., You X. Z., 2004: Continuous deformation of the Tibetan Plateau from global positioning system data. Geology **32**, 9, 809–812.

Zhang Y. J., Gao Y., Shi Y. T., Cheng W. Z., 2008: Shear-wave splitting of Sichuan regional seismic network. Acta Seismologica Sinica **21**, 2, 127–138.

Zhang Z. J., Wang Y. H., Chen Y., Houseman G. A., Tian X. B., Wang E. C., Teng J. W., 2009: Crustal structure across Longmenshan fault belt from passive source seismic profiling. Geophysical Research Letters **36**, L17310.

Zhang Z. J., Yuan X. H., Chen Y., Tian X. B., Kind R., Li X. Q., Teng J. W., 2010: Seismic signature of the collision between the east Tibetan escape flow and the Sichuan Basin. Earth and Planetary Science Letters **292**, 254–264.

Zhang Z., Yang L., Teng J., Badal J., 2011: An overview of the earth crust under China. Earth-Science Reviews, **104**, 143–166.